Contrib Mineral Petrol (2009) 158:263–281
DOI 10.1007/s00410-009-0381-x

ORIGINAL PAPER

Scale of pluton/wall rock interaction near May Lake, Yosemite National Park, CA, USA

Ryan D. Mills · Allen F. Glazner · Drew S. Coleman

Received: 25 June 2008 / Accepted: 16 January 2009 / Published online: 17 February 2009

Abstract Interaction of magma with wall rock is an important process in igneous petrology, but the mechanisms by which interactions occur are poorly known. The western outer granodiorite of the Cretaceous Tuolumne Intrusive Suite of Yosemite National Park, California, intruded a variety of metasedimentary and igneous wall rocks at 93.1 Ma. The May Lake metamorphic screen is a metasedimentary remnant whose contact zone exhibits a variety of interaction phenomena including xenolith incorporation, disaggregation, and partial melting. The chemical contrast of these metasedimentary rocks with the invading pluton provides an excellent measure of pluton/wall rock interactions. Wall rock xenoliths (mostly pelitic quartzite) are predominantly located in an elongate horizon surrounded by a hybridized fine-grained granodiorite. Initial Sr and Nd isotopic ratios of the hybridized granodiorite indicate significant local incorporation of crustal material. Major- and trace-element geochemical data indicate that contamination of the granodiorite occurred via selective assimilation of both high-K and low-K, high-silica partial melts derived from pelitic quartzite. Although the hybridized granodiorite shows significant amounts of contamination, adjacent to xenoliths the proportion of contamination is undetectable more than a meter away. These results indicate that the chemical and isotopic variability of the Tuolumne Intrusive Suite is not caused by magma contamination via in situ wall rock assimilation.

Communicated by J. Blundy.

R. D. Mills (✉) · A. F. Glazner · D. S. Coleman
University of North Carolina at Chapel Hill, Chapel Hill, NC 27599-3315, USA
e-mail: rdmills@email.unc.edu

Keywords Isotope geochemistry · Pluton emplacement · Partial melting · Sierra Nevada batholith

Introduction

Assimilation of wall rock material is commonly invoked as a cause of large-scale chemical heterogeneity in igneous rocks (McBirney et al. 1987; Clarke et al. 1998; Barnes et al. 2005; Dungan 2005) and as a space-creating mechanism for plutons in the upper crust via stoping and disaggregation (Beard et al. 2005; Dumond et al. 2005). Assimilation is an umbrella term that encapsulates both bulk incorporation of wall rock (bulk assimilation) and incorporation of partial melts of wall rocks, leaving behind a refractory residue (selective assimilation). These end-member mechanisms of assimilation produce different trends of chemical hybridization in plutons. Although several studies have defined hybridized aureoles or zones in plutons (Barnes et al. 2004; Saito et al. 2007), few detailed, meter-scale geochemical studies have identified the assimilated material and quantified the spatial extent of contamination.

Reaction of magma with wall rock is important not only for understanding magma evolution, but for quantifying large-scale geochemical fluxes. For example, the Wilson cycle dictates that passive margins sometimes are converted into subduction margins, with intrusion of magma into carbonate-rich passive margin sedimentary sequences (e.g. western North America Cordilleran, Burchfiel and Davis 1972; and the Scandinavian Caledonides, Roberts et al. 2007). Reaction of magma with limestone and dolomite can release vast quantities of carbon dioxide; thus, understanding the nature of such interaction is important to understanding geochemical cycles.

Wall rock xenoliths are rare in most plutons (typically $\ll$1% of exposed area; Glazner and Bartley 2006, 2008); thus, for incorporation of wall rocks to be a significant process in pluton evolution, assimilation of crustal material must be pervasive. Because bulk assimilation of wall rocks is a thermodynamically limited mechanism for pluton emplacement (Bowen 1928; Glazner 2007), Beard et al. (2005) suggested that plutons may dissolve and disperse up to 50% of their total mass during ascent and emplacement via reactive bulk assimilation in which a xenolith reacts and disaggregates without significant mineral dissolution. However, the chemical results of such a process would be identical to bulk assimilation because the dispersed mineral grains still reside in the magma.

Assimilation is detectable because it drives the composition of the magma toward the contaminant. If the contaminant is similar in composition to the magma, then little change results. If it is another igneous rock, then the contaminated magma will have an igneous composition as well. But if the contaminant is a non-igneous rock, then the contaminated magma will likely lie off of the well-defined igneous trend in compositional space (Fig. 1; Glazner et al. 2008). In addition, radiogenic isotopic analysis can detect assimilation if the contaminant is isotopically distinct.

This study examines chemical and physical interactions between a pluton and its wall rocks in order to determine the spatial and chemical extent of the assimilation process. We focus on the contact between granodiorite and passive

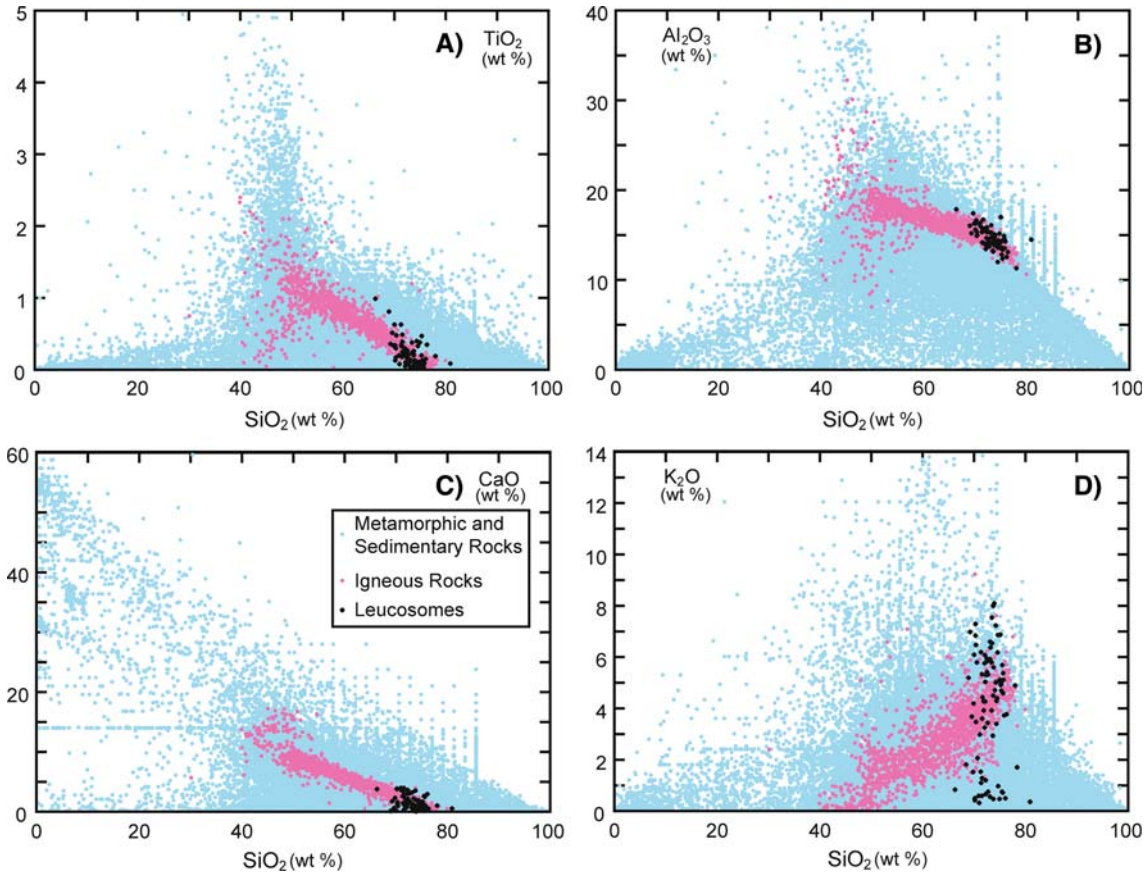

Fig. 1 Selected major-element variation diagrams of whole-rock geochemistry. Metamorphic and sedimentary rock dataset (n = 28,553, Baedecker et al. 1998) plotted with no filtering of data which leaves some semi-quantitative data in the figure (e.g. linear feature at CaO $\sim$ 14 wt.%). Mesozoic plutonic rock data from California extracted from the NAVDAT online database on 20 November 2008 (n = 1594). Leucosome data compiled from multiple sources and locations (Sawyer 1987; Bea et al. 1994; Whitney and Irving 1994; Carrington and Watt 1995; Symmes and Ferry 1995; Jung et al. 1998; Milord et al. 2001; Johnson et al. 2003; Zeng et al. 2005a; Hinchey and Carr 2006; Bhadra et al. 2007). The diagrams illustrate the large variability in whole-rock geochemistry of metamorphic and sedimentary rocks, the restricted trend of igneous rocks (volcanic rocks would plot similarly to plutonic rocks) from mafic to felsic, and the extremely restricted range of leucosome values. Leucosome values correlate with the felsic end of the plutonic trend except in the K_2O/SiO_2 plot which has two leucosome fields, with only the higher K_2O field correlating with the igneous trend. Contamination of igneous rocks by partial melts of metamorphic rocks (represented by leucosomes) would result in a rock of igneous composition (with the exception of low-K leucosomes), whereas contamination by a large number of metamorphic/sedimentary whole rocks would result in a rock with non-igneous geochemistry

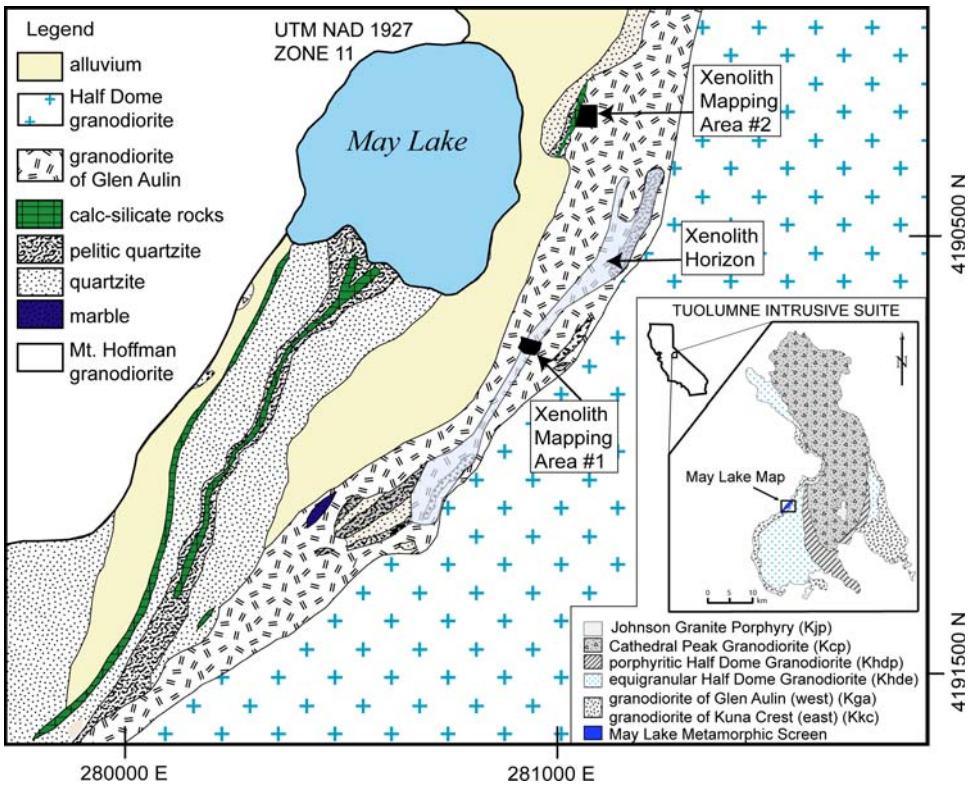

Fig. 2 Geologic map of the May Lake Metamorphic Screen (after Taylor 2003). Inset of the geologic map of the Tuolumne Intrusive Suite (after Huber et al. 1989)

margin metasedimentary wall rocks at May Lake in Yosemite National Park, California (Fig. 2), where there are abundant glaciated outcrops, great lithologic diversity of metasedimentary rocks in the wall rock screen, and significant chemical and isotopic contrasts between the pluton and the metasedimentary rocks.

Geologic background

The Tuolumne Intrusive Suite (Fig. 2) is a concentrically zoned set of plutons located in the Sierra Nevada batholith of California. The suite, which grades from granodiorite and tonalite at the margin to granodiorite in intermediate zones and granite porphyry at the core, was emplaced between 93.5 and 85.4 Ma (Coleman et al. 2004). From margin to core $^{87}Sr/^{86}Sr_{(i)}$ values rise from 0.7058 to 0.7066 and $\varepsilon Nd_{(t)}$ values drop from -3 to -6, with the most significant isotopic changes occurring near the margins of the suite (Kistler et al. 1986; Gray et al. 2008).

The May Lake metamorphic screen consists of passive margin metasedimentary rocks in contact with the western border phases of the Tuolumne Intrusive Suite (here referred to as granodiorite of Glen Aulin, Kga) for approximately 4 km (Fig. 2). The screen, mapped in detail by Rose (1957) and Taylor (2003), consists of quartzite, pelitic quartzite, marble, and calc-silicate rocks that are correlated with late Proterozoic units of the Mojave Desert region (Schweickert and Lahren 1991). Lahren et al. (1990) proposed that this assemblage of rocks originated far to the south and was transported ~400 km north along the proposed Mojave-Snow Lake fault.

Light gray to white quartzite makes up a majority of exposed metamorphic rocks in the screen and is primarily recrystallized quartz (85–95 modal %; Rose 1957) with minor biotite and potassium feldspar. Pelitic quartzite is a foliated rock with layers of relatively pure quartzite and pelitic hornfels; layer thickness typically ranges from millimeters to meters. Biotite and muscovite define a foliation in the pelitic layers and plagioclase and potassium feldspar are the other main phases. Minor phases in the pelitic quartzite include andalusite, sillimanite, and orthopyroxene (Taylor 2003). In addition, several accessory minerals are present, including apatite, zircon, monazite, and opaque minerals (Rose 1957).

The two other main metasedimentary rock types in the screen are calcareous and occur as boudins in the quartzites. The calc-silicate rock unit is an equigranular mixture of diopside, actinolite, calcite and quartz (Taylor 2003). The marble unit is coarse-grained calcite with minor diopside and actinolite (Taylor 2003). All metasedimentary rock units show evidence for pre- and syn-emplacement deformation including several episodes of folding and boudinage (Taylor 2003; Coleman et al. 2005).

The outer unit of the Tuolumne Intrusive Suite is referred to collectively as the granodiorite of Kuna Crest

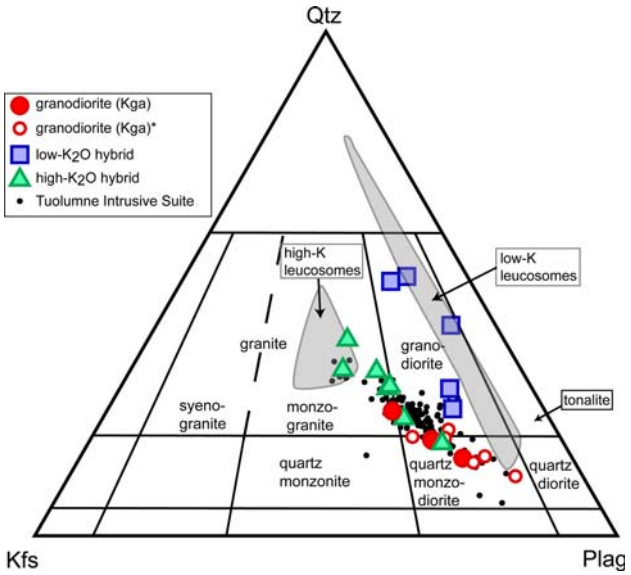

Fig. 3 Modal Quartz-Plagioclase-Potassium Feldspar compositions of plutonic rocks and leucosome geochemistry (Sawyer 1987; Bea et al. 1994; Whitney and Irving 1994; Carrington and Watt 1995; Symmes and Ferry 1995; Jung et al. 1998; Milord et al. 2001; Johnson et al. 2003 Zeng et al. 2005a; Hinchey and Carr 2006; Bhadra et al. 2007) determined using CIPW norm algorithm. Albite compositions only contribute to the plagioclase component. Rock type classifications are after Le Maitre (2002). Kga* from previous studies (Bateman et al. 1988; Gray et al. 2008)

(Kkc), but along the western edge of the suite near May Lake, the unit is specifically referred to as the tonalite of Glen Aulin (Kga). Because these rocks plot predominantly in the granodiorite field on a QAP ternary diagram (Fig. 3) the terminology used here will be granodiorite of Glen Aulin (Kga). The granodiorite is equigranular with biotite defining a subtle planar fabric. Hornblende and opaque minerals are the other major mafic phases and minor sericitization of potassium feldspar is present. Plagioclase and potassium feldspar ($An_{35–45}$ and Or_{90}; Gray 2003), along with quartz, are the main felsic constituents.

Methods

Sampling strategy

Sampling was focused largely within 10 m of the contact between the May Lake screen and the granodiorite of Glen Aulin in order to understand the scale of pluton/wall rock interactions. Previously analyzed samples of the granodiorite away from the contact were also used to define the background chemistry of the unit. Samples of each wall rock unit were collected for analysis as potential pluton contaminants. A variety of granodiorite samples was collected from within 10 m of the contact, and those samples along with two-line sampling traverses extending perpendicular from the contact were used to establish the length scale of contamination.

Xenolith mapping

Two representative areas (Fig. 2) were established for detailed mapping of xenoliths in the granodiorite: one inside a particularly xenolith-rich horizon, and the other in an area with a typical (low) density of xenoliths. A Nikon total station was used to map the location of all visible xenoliths larger than 1 cm in longest dimension. The long and short axis dimensions and rock type were noted for each xenolith within the areas.

Geochemistry

Samples were ground to a powder using a steel jaw crusher and a ceramic shatterbox. Powders were then shipped to Activation Laboratories (Ontario, Canada), for major- and trace-element analyses. Samples were dissolved by lithium metaborate/tetraborate fusion. Major-elements and Sc, Be, V, Sr, Zr, and Ba were analyzed by ICP–OES and all other trace-elements were analyzed by ICP–MS.

Isotope geochemistry

Whole-rock powder was dissolved and cations were separated for isotopic analysis following methods outlined by Miller et al. (1995). Strontium and Nd isotopic abundances were obtained on a VG Sector 54 thermal ionization mass spectrometer at the University of North Carolina at Chapel Hill. Strontium isotopic ratios were normalized to $^{86}Sr/^{88}Sr = 0.1194$ and referenced to $^{87}Sr/^{86}Sr = 0.710266$ (NBS 987, $n = 9$); Nd isotopic ratios were normalized to $^{146}Nd/^{144}Nd = 0.7219$ and referenced to $^{143}Nd/^{144}Nd = 0.512117$ (JNdi-metal, $n = 4$). Isotope dilution using spikes was not performed because Rb, Sr, Sm and Nd concentrations were obtained via ICP–MS. $^{87}Sr/^{86}Sr_{(i)}$ and $\varepsilon Nd_{(t)}$ indicate values corrected to 93.1 Ma, the crystallization age of the granodiorite (Coleman et al. 2004). Epsilon values for Nd were calculated using $^{143}Nd/^{144}Nd$ (CHUR, 0 Ma) = 0.512638 and $^{147}Sm/^{144}Nd$(CHUR, 0 Ma) = 0.1967.

Heavy mineral separates

One hundred grams blocks of three samples (ML051.02, ML051.03, & ML061.63) were reduced to sand size using a Bico disc mill. Highly magnetic minerals were removed from the samples with a hand magnet. Remaining minerals were passed through methelyne iodide with a density of

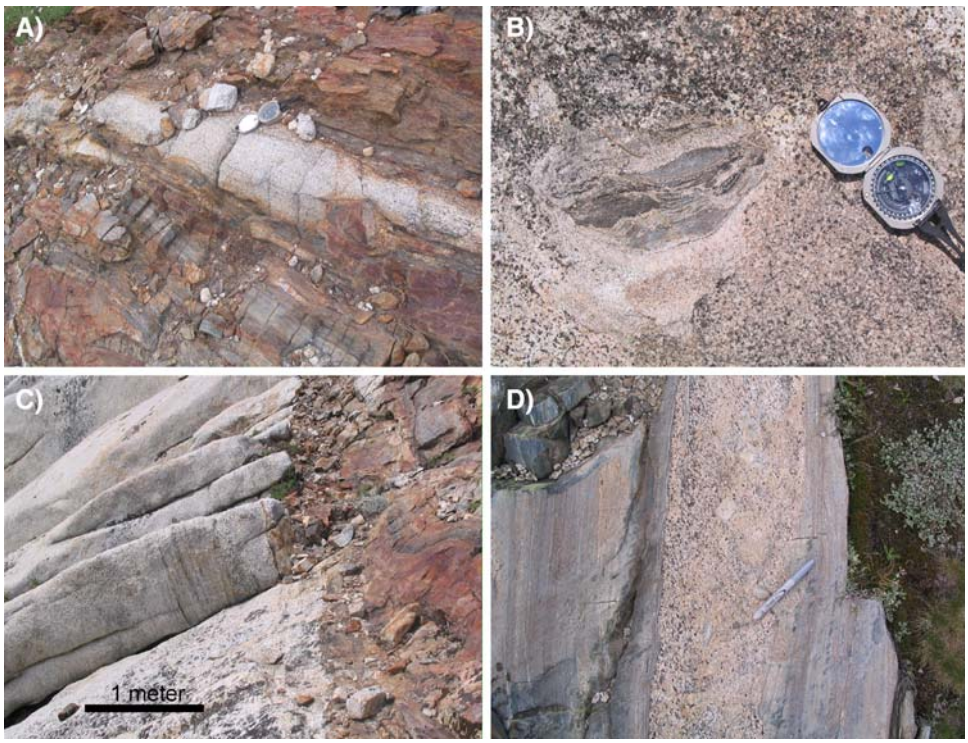

Fig. 4 Field photographs of interactions between plutonic rocks and metamorphic wall rocks. **a** A concordant intrusion of hybridized granodiorite in the pelitic quartzite, sample ML061.36 was collected from the center of the granodiorite dike. **b** A pelitic quartzite xenolith surrounded by a leucocratic rind. **c** A contact between granodiorite and a large block of mixed metasedimentary rock type. Modal layering in the granodiorite is prominent parallel to the block contact. **d** A concordant intrusion of granodiorite in foliated metavolcanic rocks on the eastern side of the Tuolumne Intrusive Suite

3.32 g/cm^3 to segregate dense minerals. Heavy mineral separates were mounted in epoxy, polished, and identified using energy-dispersive X-ray analysis on a Leica SEM with special attention paid to rare earth element-(REE) and Th-bearing phases.

Results

Field relationships

The May Lake screen is approximately 4,500 m in length and 550 m in width. Each of the four major metasedimentary rock units is locally in contact with the granodiorite but only pelitic quartzite, the only foliated metasedimentary unit, displays evidence of concordant dike injections resulting in isolation of metasedimentary blocks (Fig. 4a).

Xenoliths in the granodiorite around May Lake occur predominantly in a tabular zone that is approximately 1,100-m long and 200-m wide and strikes subparallel to the contact between the screen and granodiorite. Xenoliths in the zone range in size from a few square centimeters to a single large block, 140 m × 240 m in area, near the contact (Taylor 2003). Hybridized, fine-grained granodiorite surrounds most xenoliths in the tabular xenolith zone (Fig. 4b) and the hybridized granodiorite has a lower abundance of mafic minerals than the typical granodiorite. Xenoliths found in the hybridized zone are chiefly pelitic quartzite and show more ductile deformation than xenoliths outside of the zone. Granodiorite immediately surrounding the xenolith zone has modally layered bands defined by mafic minerals that are parallel to the edge of the zone (Fig. 4c). In contrast, xenolith-free zones of the granodiorite have little to no modal layering.

Mapping of xenoliths in the xenolith horizon illustrates the contrast between the horizon and surrounding granodiorite. Mapping area #1 (Figs. 2, 5) consisted of a 40 m × 20 m area of excellent exposure chosen to encompass the xenolith-rich horizon which is approximately 10–15 m thick and is surrounded by typical

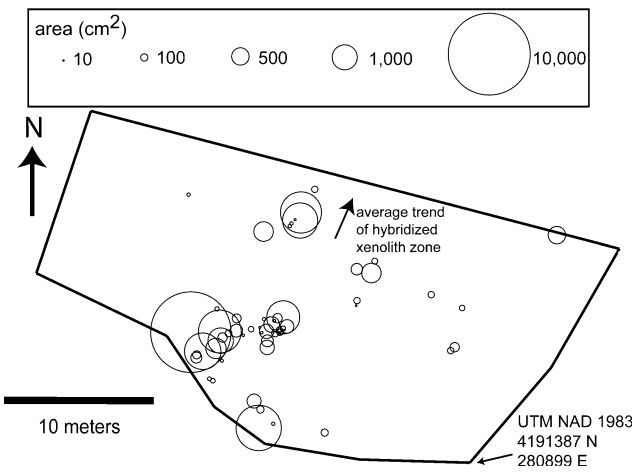

Fig. 5 Representation of xenoliths mapped in zone 1. *Circles* are proportional to xenolith area, elliptical area calculated from long and short axis field measurements

Table 1 Whole-rock major-element concentrations (wt.%)

Sample name	SiO_2	TiO_2	Al_2O_3	Fe_2O_3(T)	MnO	MgO	CaO	Na_2O	K_2O	P_2O_5	LOI	Total
Granodiorite												
ML051.04	67.63	0.513	15.56	3.96	0.061	1.67	3.45	3.17	4.04	0.15	0.370	100.60
ML061.61	60.23	0.741	17.35	5.96	0.099	2.54	5.50	3.69	2.71	0.22	1.159	100.20
ML061.63	61.54	0.764	16.25	5.75	0.089	2.43	4.78	3.28	3.20	0.22	1.189	99.50
Hybridized granodiorite												
ML051.02 (L)	77.86	0.331	11.17	1.95	0.031	0.73	2.55	2.53	1.61	0.08	0.444	99.29
ML051.08 (H)	66.62	0.517	15.73	4.42	0.062	1.72	3.86	3.33	3.81	0.17	0.347	100.60
ML051.18 (L)	64.38	0.863	16.54	5.58	0.068	2.45	4.39	3.41	2.28	0.23	0.506	100.70
ML061.25 (L)	66.56	0.852	15.67	4.62	0.053	1.95	4.10	3.40	2.10	0.19	1.075	100.60
ML061.26 (H)	62.06	0.785	16.74	5.89	0.088	2.49	5.01	3.46	3.04	0.23	0.905	100.70
ML061.28 (H)	76.69	0.137	12.81	1.17	0.020	0.34	1.90	2.65	4.36	0.06	0.392	100.50
ML061.30 (H)	72.00	0.194	15.43	1.61	0.031	0.50	2.77	3.43	4.03	0.08	0.448	100.50
ML061.36 (L)	75.68	0.393	12.49	2.32	0.029	1.05	2.64	2.13	2.05	0.05	1.426	100.30
ML061.38 (H)	64.88	0.975	14.97	6.29	0.107	2.74	3.23	2.23	3.43	0.26	1.325	100.40
ML061.40 (H)	67.49	0.591	14.78	4.35	0.054	1.61	3.07	2.93	3.60	0.15	1.157	99.79
ML061.60 (L)	72.59	0.410	13.93	2.67	0.043	1.22	3.64	3.12	1.17	0.08	1.153	100.00
Quartzite												
ML051.14	91.61	0.064	4.64	1.20	0.021	0.54	0.18	0.15	1.31	0.09	0.368	100.20
ML061.37	89.14	0.195	5.81	0.47	0.011	0.10	0.27	0.83	3.26	0.02	0.319	100.40
ML061.39	94.82	0.083	2.13	0.73	0.006	0.14	0.09	0.24	0.90	0.04	0.442	99.63
Pelitic quartzite												
ML051.03	81.44	0.600	7.68	3.48	0.054	1.34	0.92	1.30	2.90	0.14	0.348	100.20
ML061.29	67.30	0.791	15.93	3.86	0.130	1.81	7.14	1.22	1.15	0.10	1.134	100.60
calc-silicate rocks												
ML051.17	48.74	0.511	14.52	7.73	0.440	6.18	21.68	0.39	0.07	0.10	0.239	100.10
ML061.59	50.93	0.665	15.94	6.14	0.356	8.42	15.82	0.47	0.52	0.09	1.024	100.40
Marbles												
ML051.05	34.83	0.028	0.59	1.02	0.200	1.54	47.47	0.02	<0.01	0.97	13.910	100.60
ML-85	15.11	0.061	0.82	0.88	0.061	4.35	48.00	0.02	0.02	0.07	31.240	100.60

Table 1 continued

Whole-rock trace-element concentrations (ppm)																					
Sample name	Sc	Be	V	Cr	Co	Ni	Cu	Zn	Ga	Ge	As	Rb	Sr	Y	Zr	Nb	Mo	Ag	In	Sn	Sb	Cs
Granodiorite																						
ML051.04	6	2	77	<20	9	<20	<10	50	16	1.1	<5	172	422	8	156	4.5	<2	<0.5	<0.1	<1	0.4	7.8
ML061.61	12	2	123	<20	14	<20	<10	70	21	1.3	5	131	523	32.2	191	8.8	<2	<0.5	<0.1	2	<0.2	9.2
ML061.63	11	2	124	<20	14	<20	<10	70	19	1.3	6	150	500	18.6	165	6.9	<2	<0.5	<0.1	1	0.8	7.2
Hybridized granodiorite																						
ML051.02 (L)	2	1	41	<20	5	<20	20	<30	12	0.9	6	90	261	6.9	350	3.2	<2	<0.5	<0.1	<1	0.4	6.9
ML051.08 (H)	12	2	87	<20	8	<20	30	50	16	1.1	5	141	435	30.2	157	7.7	<2	<0.5	<0.1	<1	0.4	6.7
ML051.18 (L)	7	2	129	<20	12	<20	20	60	19	1	<5	168	411	5.1	198	8.1	<2	<0.5	<0.1	<1	0.6	13.4
ML061.25 (L)	4	2	117	<20	10	<20	40	60	17	0.9	<5	134	439	15.4	150	8.2	<2	<0.5	<0.1	1	0.4	7.7
ML061.26 (H)	11	2	125	<20	13	<20	20	60	18	1	<5	141	508	9.6	165	5.3	<2	<0.5	<0.1	<1	0.4	7.3
ML061.28 (H)	1	1	21	<20	2	<20	<10	<30	11	1	<5	122	352	3.5	77	2.5	<2	<0.5	<0.1	<1	0.3	8.3
ML061.30 (H)	1	1	25	<20	4	<20	<10	970	16	1.1	<5	130	466	2.8	91	3	<2	<0.5	<0.1	<1	<0.2	6.9
ML061.36 (L)	6	1	43	<20	7	<20	<10	<30	15	1.1	<5	83	215	13.7	169	9.3	3	<0.5	<0.1	<1	<0.2	3.6
ML061.38 (H)	13	1	151	<20	14	<20	<10	80	21	1.4	6	256	155	22.5	201	17.6	4	<0.5	<0.1	3	0.3	18.1
ML061.40 (H)	3	2	90	<20	9	<20	<10	50	18	1	<5	175	356	3.8	177	3.6	<2	<0.5	<0.1	<1	<0.2	8.2
ML061.60 (L)	4	2	46	<20	7	<20	30	40	17	1.1	<5	109	318	4.5	175	6.8	<2	<0.5	<0.1	<1	<0.2	12.7
Quartzite																						
ML051.14	1	<1	6	<20	3	<20	<10	<30	5	1	23	25	18	12.6	31	1.1	<2	<0.5	<0.1	<1	0.3	1
ML061.37	1	<1	11	<20	<1	<20	<10	<30	5	0.9	<5	97	45	2.8	161	4.2	6	<0.5	<0.1	<1	<0.2	3.3
ML061.39	<1	<1	13	<20	3	<20	60	<30	3	0.7	5	33	24	3.9	359	1.3	<2	<0.5	<0.1	<1	3.9	1.5
Pelitic quartzite																						
ML051.03	6	1	38	40	5	20	10	30	10	0.9	<5	123	30	26.8	507	8.2	<2	<0.5	<0.1	<1	0.3	8.3
ML061.29	11	2	78	80	2	<20	60	40	18	1	26	61	108	19.3	190	14	<2	<0.5	<0.1	<1	0.3	6
calc-silicate rocks																						
ML051.17	13	3	61	60	11	30	60	130	19	1.5	12	8	151	34.2	150	13.4	2	<0.5	<0.1	6	0.8	1.7
ML061.59	14	3	80	80	9	40	<10	80	23	2.1	<5	33	214	37.4	166	14.8	<2	<0.5	<0.1	2	<0.2	1.8
Marbles																						
ML051.05	<1	<1	27	<20	<1	<20	<10	<30	1	<0.5	47	<1	94	8.6	12	2	<2	<0.5	<0.1	<1	0.7	<0.1
ML-85	1	<1	6	<20	<1	<20	<10	<30	1	<0.5	<5	<1	279	5.9	106	1.8	<2	<0.5	<0.1	<1	0.4	0.1

Table 1 continued

Whole-rock trace-element concentrations (ppm)																						
Sample name	Ba	La	Ce	Pr	Nd	Sm	Eu	Gd	Tb	Dy	Ho	Er	Tm	Yb	Lu	Hf	Ta	W	Tl	Pb	Bi	Th	U
Granodiorite																							
ML051.04	993	14.9	28	2.78	9.91	1.84	0.665	1.49	0.24	1.33	0.26	0.77	0.125	0.88	0.147	4.2	0.43	<0.5	0.91	28	0.1	55.3	12.4
ML061.61	824	24.7	61.6	7.62	30.7	6.36	1.46	5.37	0.94	5.28	1.02	3.16	0.514	3.36	0.482	5.5	1.65	1.1	0.7	13	0.2	22.7	9.67
ML061.63	861	26.6	55.1	5.95	22.8	4.32	1.12	3.5	0.58	3.25	0.63	1.79	0.26	1.63	0.249	4.8	0.56	0.7	0.82	14	0.2	30.9	8.11
Hybridized granodiorite																							
ML051.02 (L)	275	122	213	18.8	57.6	6.09	0.795	3.34	0.32	1.4	0.24	0.71	0.106	0.76	0.137	9.6	0.3	0.5	0.51	13	0.2	74.6	12.1
ML051.08 (H)	1125	15.6	40.2	5.47	24.4	5.91	1.05	5.28	0.93	5.42	1.01	2.84	0.419	2.57	0.366	4.6	0.8	<0.5	0.78	15	0.1	29.4	5.82
ML051.18 (L)	326	32.7	56.9	5.49	17.4	2.34	1.04	1.69	0.21	0.99	0.18	0.51	0.074	0.51	0.091	5.2	0.34	2.7	1.04	10	0.1	13.1	4.39
ML061.25 (L)	379	28.2	52.4	6.37	23.5	4.11	1.3	3.36	0.51	2.65	0.49	1.46	0.218	1.39	0.215	4.3	1.59	3.4	0.8	10	0.2	17	7.73
ML061.26 (H)	858	19	36.6	3.71	13.1	2.48	0.864	2.03	0.32	1.81	0.34	0.96	0.143	0.97	0.151	4.5	0.38	4.6	0.75	17	0.9	18.6	5.19
ML061.28 (H)	1127	8.52	12.6	1.08	3.43	0.56	0.382	0.45	0.08	0.52	0.11	0.35	0.061	0.48	0.081	2.6	0.37	<0.5	0.66	21	0.1	11.4	4.54
ML061.30 (H)	1054	12.9	18.1	1.42	4.26	0.66	0.485	0.42	0.07	0.41	0.08	0.26	0.044	0.35	0.064	2.8	0.3	<0.5	0.64	21	0.2	21.7	5.28
ML061.36 (L)	330	62.1	127	13.2	47.7	7.65	1.17	5.48	0.75	3.21	0.5	1.17	0.136	0.76	0.103	5.3	0.64	1	0.47	15	<0.1	59.4	3.36
ML061.38 (H)	358	14.9	32.2	3.68	15.1	3.53	0.894	3.32	0.64	4.02	0.78	2.26	0.33	2.05	0.297	5.6	1.19	3.3	1.74	15	0.1	8.48	2.96
ML061.40 (H)	640	10.4	17.4	1.75	6.68	1.19	0.615	0.97	0.14	0.72	0.13	0.36	0.052	0.37	0.063	5.2	0.13	<0.5	0.94	15	<0.1	29.1	5.13
ML061.60 (L)	131	12.9	19.2	1.96	6.51	1.04	0.689	0.85	0.13	0.73	0.15	0.44	0.072	0.53	0.089	5.7	0.6	<0.5	0.62	9	0.1	34.7	13.4
Quartzite																							
ML051.14	195	10.5	22.7	2.39	9.06	1.92	0.512	1.82	0.34	2.08	0.43	1.31	0.199	1.28	0.189	0.9	0.16	<0.5	0.16	<5	0.6	2.78	2.25
ML061.37	382	7.92	14.3	1.38	4.56	0.72	0.374	0.5	0.08	0.42	0.09	0.28	0.047	0.35	0.061	4.4	0.35	2.8	0.47	19	0.1	9.68	2.81
ML061.39	94	23.6	44.8	3.98	13.1	1.63	0.146	1.03	0.14	0.67	0.13	0.41	0.067	0.52	0.097	11.8	0.09	0.5	0.21	5	0.1	127	19.1
Pelitic quartzite																							
ML051.03	312	42.4	101	9.97	37.1	6.86	1.22	5.89	0.94	4.94	0.93	2.73	0.384	2.35	0.373	12.2	0.69	1.2	0.74	9	<0.1	18.7	2.01
ML061.29	130	16.8	42.1	4.65	19.3	4.32	1.13	4.1	0.73	4	0.71	1.93	0.261	1.6	0.236	5	1.42	<0.5	0.41	6	<0.1	10.5	2.28
calc-silicate rocks																							
ML051.17	22	36.5	85.3	9.54	37	7.28	1.86	6.64	1.13	6.22	1.15	3.21	0.468	2.98	0.453	3.9	1.23	19.3	<0.05	<5	0.2	10.2	4.65
ML061.59	337	52.1	107	11.5	42.4	7.62	1.58	6.51	1.14	6.38	1.24	3.74	0.575	3.7	0.516	4.9	1.38	<0.5	0.17	<5	0.2	16.6	3.35
Marbles																							
ML051.05	8	5.27	7.93	1.04	4.03	0.74	0.301	0.77	0.12	0.69	0.15	0.49	0.074	0.45	0.067	0.3	0.11	<0.5	<0.05	8	6.4	0.9	9.82
ML-85	16	5.59	13.3	1.31	4.93	1.02	0.263	0.89	0.16	0.94	0.18	0.55	0.087	0.59	0.098	2.7	0.11	1	<0.05	8	<0.1	2.52	1.48

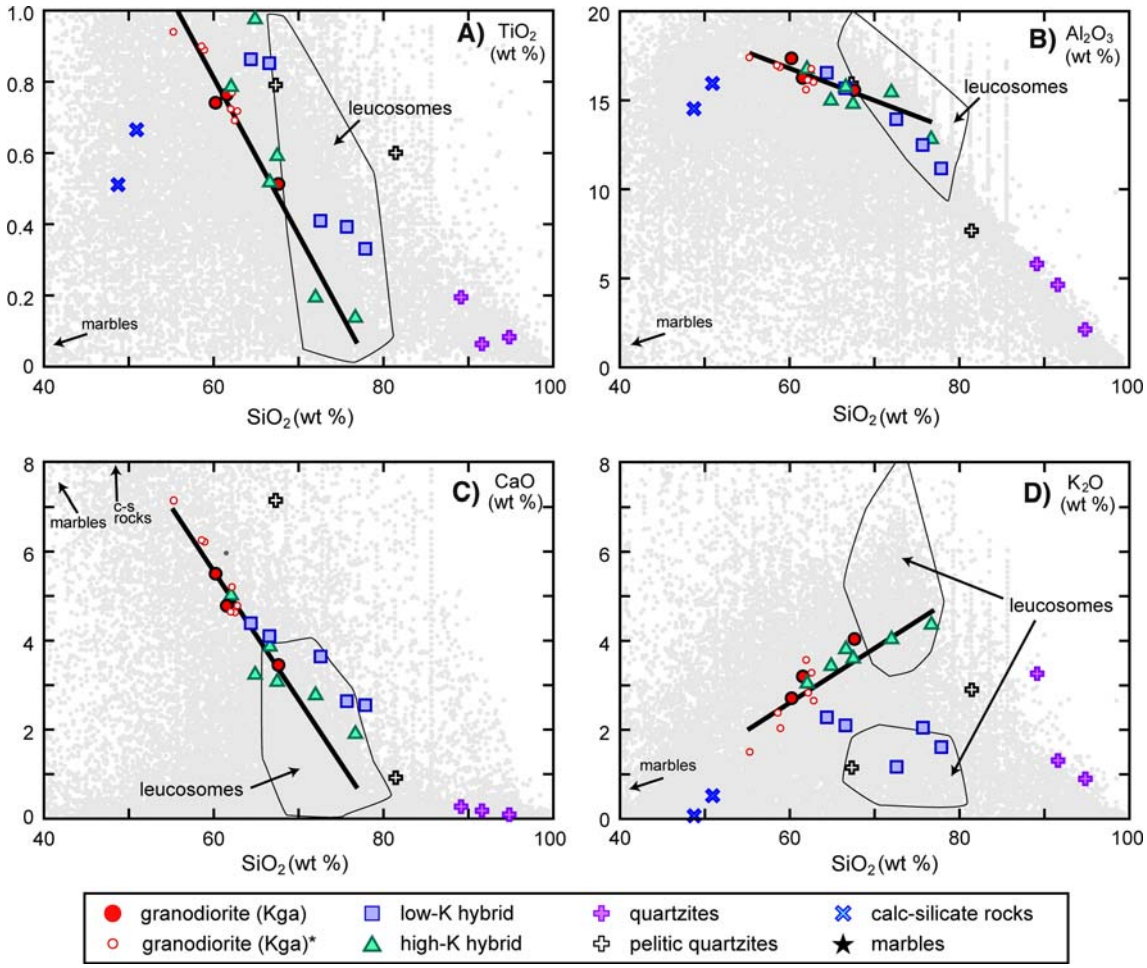

Fig. 6 Selected major-element variation diagrams of whole-rock geochemistry from this study. *Light gray dots* represent the igneous, metamorphic and sedimentary whole-rock data from Fig. 1. *Black line* is the best fit line of data from the Tuolumne Intrusive Suite (Bateman et al. 1988; Gray et al. 2008), data are shown in Fig. 13 for reference. Fields for leucosomes were drawn from data in Fig. 1. Kga* from previous studies (Bateman et al. 1988; Gray et al. 2008)

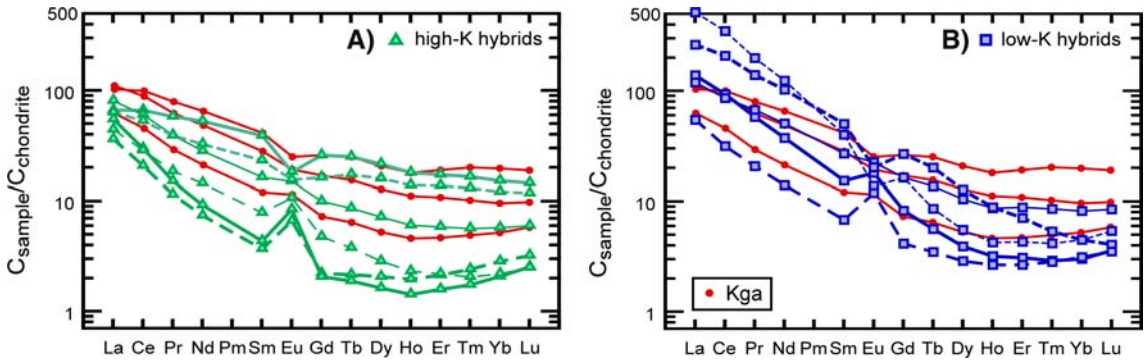

Fig. 7 Rare-earth element geochemistry of plutonic rocks plotted relative to chondrite (Sun and McDonough 1989). *Plot A* displays the high-K hybridized samples and *plot B* displays the low-K hybridized samples

xenolith-poor granodiorite. Although xenoliths account for ~2.5% of the 800 m^2 area surveyed, within the xenolith-rich horizon in this mapping area, xenoliths make up 10.5% by area, illustrating the subjectivity of quantifying xenolith abundances. In the second mapping area (Fig. 2), adjacent to the contact with calc-silicate rocks, xenoliths make up 0.005% of the 1,050 m^2 area, with all xenoliths occurring within 10 m of the contact.

Major- and trace-element geochemistry

Major and trace-element data are presented in Table 1. Plutonic rock samples with Sr and Nd isotopic ratios within the range of values from previously reported standard Kga samples (Kistler et al. 1986; Gray et al. 2008) are denoted "granodiorite." Plutonic rock samples with $^{87}Sr/^{86}Sr_{(i)}$ values higher and $\varepsilon Nd_{(t)}$ values lower than standard Kga are denoted "hybridized granodiorite."

Among granodiorite samples all major-element concentrations (Fig. 6) negatively correlate with SiO_2 (55–68 wt.%) except K_2O, which correlates positively, and Na_2O, which shows no correlation. Rubidium, Ba, and Zr correlate positively with SiO_2, whereas Sr, Zn, V, and Sc negatively correlate. Chondrite-normalized rare-earth element concentrations for granodiorite show light rare earth element (LREE) enrichment with values averaging ~100

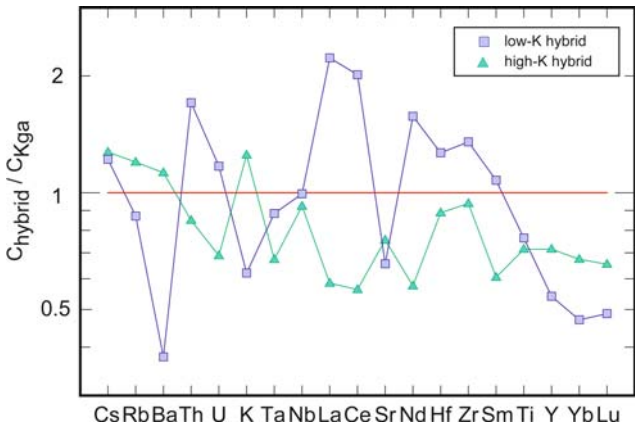

Fig. 8 Trace-element variation diagram displaying averages of the low-K hybrids and high-K hybrids normalized relative to the average of Kga. The two groups of hybrids exhibit major differences for trace-elements such as Ba, Th, and all REE

Table 2 Whole-rock Sr and Nd isotopic data

Sample name	$^{143}Nd/^{144}Nd$	±2s	$\varepsilon Nd_{(t)}$	[Nd]	[Sm]	$^{87}Sr/^{86}Sr$	± 2s	$^{87}Sr/^{86}Sr_i$	[Sr]	[Rb]
Granodiorite										
ML051.04	0.512410	0.000012	−3.45	9.9	1.8	0.707384	0.000008	0.705802	422	172
ML061.61	0.512405	0.000009	−3.70	30.7	6.4	0.706907	0.000010	0.705935	523	131
ML061.63	0.512394	0.000010	−3.78	22.8	4.3	0.706959	0.000007	0.705795	500	150
Hybridized granodiorite										
ML051.02 (L)	0.512286	0.000012	−5.29	57.6	6.1	0.707678	0.000008	0.706340	261	90
ML051.08 (H)	0.512403	0.000008	−3.99	24.4	5.9	0.707363	0.000007	0.706105	435	141
ML051.18 (L)	0.512273	0.000010	−5.75	17.4	2.3	0.708775	0.000006	0.707189	411	168
ML061.25 (L)	0.512400	0.000007	−3.56	23.5	4.1	0.707818	0.000008	0.706633	439	134
ML061.26 (H)	0.512428	0.000044	−3.13	13.1	2.5	0.707569	0.000007	0.706492	508	141
ML061.28 (H)	0.512240	0.000023	−6.61	3.4	0.6	0.707823	0.000008	0.706478	352	122
ML061.30 (H)	0.512257	0.000014	−6.20	4.3	0.7	0.707307	0.000009	0.706224	466	130
ML061.36 (L)	0.512089	0.000006	−9.52	47.7	7.7	0.715645	0.000007	0.714147	215	83
ML061.38 (H)	0.512067	0.000006	−10.48	15.1	3.5	0.717084	0.000007	0.710674	155	256
ML061.40 (H)	0.512341	0.000013	−4.73	6.7	1.2	0.708109	0.000007	0.706201	356	175
ML061.60 (L)	0.512179	0.000097	−7.76	6.5	1.0	0.708401	0.000007	0.707071	318	109
Quartzite										
ML051.14	0.511475	0.000023	−21.89	9.1	1.9	0.765441	0.000007	0.760051	18	25
ML061.37	0.511646	0.000028	−18.15	4.6	0.7	0.722843	0.000007	0.714478	45	97
ML061.39	0.512157	0.000007	−7.95	13.1	1.6	0.711588	0.000007	0.706252	24	33
Pelitic quartzite										
ML051.03	0.511373	0.000010	−23.67	37.1	6.9	0.789945	0.000007	0.774034	30	123
ML061.29	0.511917	0.000048	−13.35	19.3	4.3	0.732385	0.000007	0.730193	108	61
calc-silicate rocks										
ML051.17	0.511635	0.000025	−18.65	37.0	7.3	0.728369	0.000007	0.728164	151	8
ML061.59	0.511625	0.000008	−18.72	42.4	7.6	0.748255	0.000008	0.747656	214	33
Marbles										
ML051.05						0.710385	0.000007	0.710344	94	1
ML-85	0.511750	0.000018	−16.47	4.9	1.0	0.710961	0.000007	0.710947	279	1

times chondrite for La (Fig. 7). A few samples show minor positive and negative Eu anomalies, but as a whole, the granodiorite has negligible Eu anomalies.

Hybridized granodiorite samples are generally peraluminous and have higher concentrations of SiO_2 (62–78 wt.%) than granodiorite samples and diverge into two groups when correlated with K_2O. One group, hereafter referred to as high-K, has a positive correlation between SiO_2 and K_2O, following the trend of the entire Tuolumne Intrusive Suite (Fig. 6). The other, referred to as low-K, has a negative correlation between SiO_2 and K_2O, and K_2O concentrations are predominantly <2 wt.% for rocks in this group. Barium concentrations differ between groups (Fig. 8), with high-K samples having high Ba concentrations (~1,000 ppm) and low-K samples having lower Ba concentrations (<400 ppm). Low-K samples can have higher LREE concentrations (Figs. 7, 8) than high-K and granodiorite samples. Several of the hybridized samples have large Eu anomalies, some positive and some negative, but there is no direct correlation between the groups defined by K_2O concentrations and the sign or intensity of Eu anomalies.

Metasedimentary rocks found in the screen span a large range of major-element compositions (Fig. 6). The quartzite has measured SiO_2 values between 88 and 95 wt.% with variable amounts of Al_2O_3 and K_2O making up most of the remainder. Outcrops of the quartzite are massive with weak foliation, in contrast to the well-foliated pelitic quartzite. The composition of the pelitic quartzite varies depending on the relative abundance of silt to sand layers in the protolith, with SiO_2 ranging from 67 to 81 wt.%. The calc-silicate rock unit has SiO_2 concentrations around 50 and 6–9 wt.% MgO. The marble varies in purity, but both analyzed samples have ~48 wt.% CaO before degassing.

Sr and Nd isotope geochemistry

Whole-rock Nd and Sr isotope ratios are presented in Table 2. $^{87}Sr/^{86}Sr_{(i)}$ and $\varepsilon Nd_{(t)}$ are corrected to the crystallization age of the granodiorite of Glen Aulin (93.1 Ma). Granodiorite away from the screen exhibits a range of $\varepsilon Nd_{(t)}$ from −3.43 to −3.78 and $^{87}Sr/^{86}Sr_{(i)}$ from 0.705795 to 0.705935 (Kistler et al. 1986; Gray et al. 2008; this study). Hybridized granodiorite ranges in $\varepsilon Nd_{(t)}$ from −3.54 to −10.46 and $^{87}Sr/^{86}Sr_{(i)}$ from 0.706105 to 0.714147, and $\varepsilon Nd_{(t)}$ and $^{87}Sr/^{86}Sr_{(i)}$ correlate throughout the hybridized granodiorite samples (Fig. 9). All granodiorite samples with hybridized compositions were collected within 2 m of wall rock material and all samples farther from the wall rocks show no isotopic variation from the granodiorite. Plots of distance from wall rock versus isotopic ratios (Fig. 10) show the dramatic decrease in isotopic heterogeneity as distance from wall rock increases. A plot of $\varepsilon Nd_{(t)}$

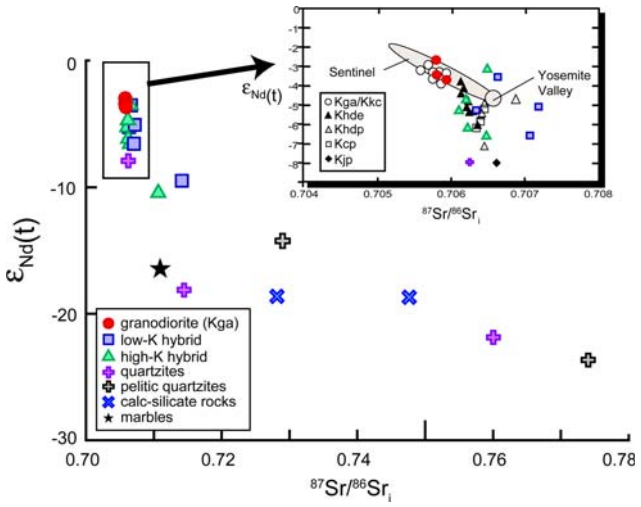

Fig. 9 Plot of $\varepsilon Nd_{(t)}$ against $^{87}Sr/^{86}Sr_{(i)}$, both corrected to 93.1 Ma. Wall rocks span a large isotopic range whereas granodiorite samples define a small range. The hybridized samples spread from the granodiorite toward the wall rocks. Inset plot shows all units of the Tuolumne Intrusive Suite (Gray et al. 2008) and fields for the Sentinel (Kistler et al. 1986; Coleman and Glazner 1997) and Yosemite Valley (Ratajeski 1999) plutonic units

versus K_2O (Fig. 11) clearly differentiates the two contamination trends in the hybridized granodiorite samples, with one contaminant having high K_2O (~5 wt.%) and the other contaminant having low K_2O (<1 wt.%).

The potential contaminants all have more radiogenic Sr isotopic ratios and less radiogenic Nd isotopic ratios than the granodiorite, with $\varepsilon Nd_{(t)}$ ranging from −7.92 to −23.65 for both types of quartzites, and approximately equal to −18 for calc-silicate rocks and −16 for marbles. The variability in isotopic ratios and daughter isotope whole-rock concentrations produces a great variety of potential mixing trends between the granodiorite and varied metasedimentary wall rocks.

Trace mineralogy

Semi-quantitative observations of heavy mineral separates are summarized in Table 3. Monazite is the only observed phase in the pelitic quartzite sample (ML051.03) with significant concentrations of LREE and Th. Allanite is the only observed phase with significant concentrations of LREE in the plutonic rock samples and uranothorite is the only observed phase with significant concentrations of Th in the plutonic rock samples. However, the relative abundances of allanite and thorite are higher in the hybridized sample (ML051.02) than they are in the granodiorite sample (ML061.63). Although monazite, allanite, and uranothorite have the highest concentrations of LREE and Th, the remaining minerals in the rock house the majority of these elements.

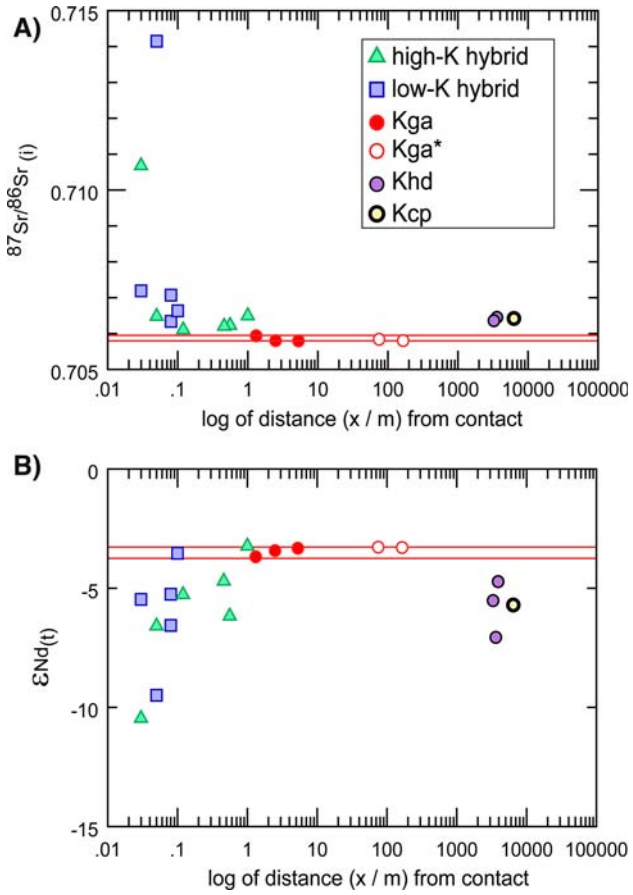

Fig. 10 Plot A and B show the isotopic variability of Sr and Nd in the plutonic rocks relative to distance from wall rock material. Selected inner unit samples (Gray et al. 2008) with the May Lake metamorphic screen as their closest wall rock in map view are also plotted

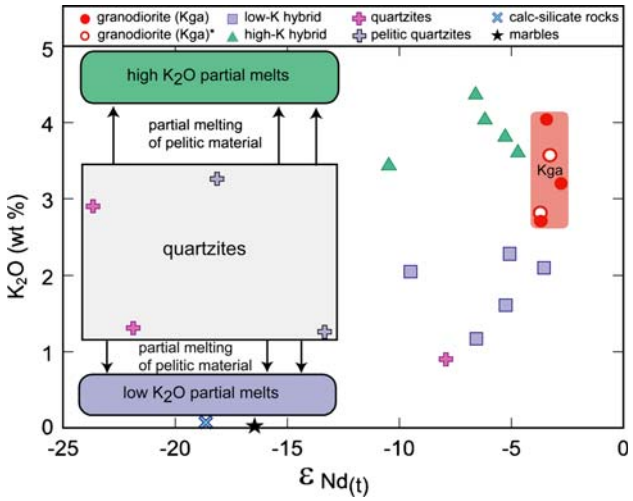

Fig. 11 Plot of $\varepsilon Nd_{(t)}$ corrected to 93.1 Ma versus K_2O (wt.%) illustrating two trends in contamination of Kga. One trend has increased K_2O as $\varepsilon Nd_{(t)}$ gets more negative and the other has decreased K_2O as $\varepsilon Nd_{(t)}$ gets more negative. Partial melting can produce two distinct chemical compositions while $\varepsilon Nd_{(t)}$ stays relatively constant, because these melting reactions do not significantly fractionate Sm from Nd

Table 3 Heavy mineral separates elemental data

Sample name	Pelitic quartzite ML051.03	Hybridized granodiorite ML051.02	Granodiorite ML061.63
Monazite percent of heavy minerals	~10%		
Uranothorite percent of heavy minerals		~3%	<1%
Allanite percent of heavy minerals		~15%	<1%
Ce in monazite (ppm)	~15		
Th in monazite (ppm)	~3		
Ce in allanite (ppm)		~18	<3
Th in uranothorite (ppm)		~27	<18
Ce in whole-rock (ppm)	101	213	55
Th in whole-rock (ppm)	19	75	31
Heavy minerals/total	0.05 wt.%	0.2 wt.%	0.4 wt.%

Heavy mineral separates contain minerals that passed through MEI liquid with a density of 3.2 g/cm^3

Mineral percentages were estimated by point counts of heavy mineral mounts using energy dispersive spectrometry (EDS) on a SEM

Mixing percentages

Weighted least-squares analysis of major-element concentrations was performed to estimate percentages of the granodiorite component and the contaminant component in the hybridized samples. Average major-element concentrations of Kga were used as one end-member of mixing and averages of leucosome analyses (divided into low-K and high-K groups; Fig. 1) were used as the other end-members of mixing. The low-K_2O contaminant was used for hybridized samples that have lower K_2O weight percents than the average granodiorite and the high-K_2O contaminant was used for hybridized samples that have higher K_2O weight percents than the average granodiorite. Calculations for individual hybridized samples produced mixing percentages ranging from ~0% wall rock contaminated to ~100% wall rock contaminated (Fig. 12), with highly contaminated samples occurring within 10 cm of the wall rock.

Discussion

Xenoliths

Xenoliths observed in the granodiorite are overwhelmingly pelitic quartzite (~90%, determined from xenolith mapping) and metamorphic residue interpreted as restite from pelitic quartzite based on field interpretations. However, the metasedimentary screen contains only ~5 area % pelitic quartzite, with the remaining ~95 area % consisting

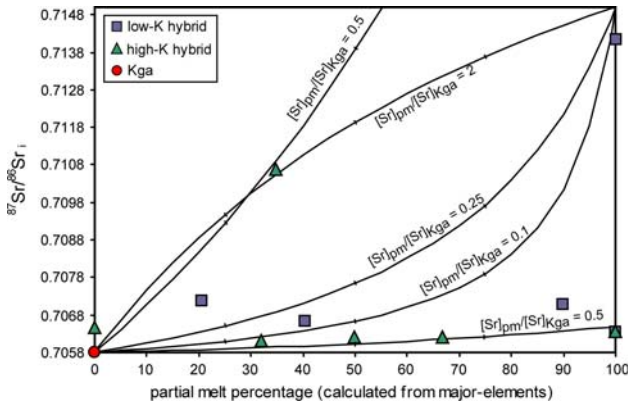

Fig. 12 $^{87}Sr/^{86}Sr_{(i)}$ values for average Kga and hybridized granodiorite samples plotted against results from weighted least-squares mixing analysis of major-element chemistry. Mixing hyperbolas are not shown as quantifiable mixing percentages. Mixing hyperbolas are shown for several wall rock partial melt scenarios to illustrate: (1) the variability in isotopic ratio of the quartzites in the screen (shown are three examples: 0.730, 0.715, and 0.7065), and (2) the variability in mixing paths dependent on Sr concentrations in the partial melts. Disequilibrium melting of the pelitic quartzite would produce even more possibilities for mixing. Tick marks on the mixing paths represent 25, 50, and 75%

of massive wall rock units (quartzite, marble, calc-silicate rocks; Fig. 2) as estimated from Taylor's (2003) map of the area. Thus, observed xenolith abundances do not conform to wall rock abundances in the May Lake screen. Physical properties of the wall rock such as foliation, and chemical properties such as mineral fertility for partial melting, play an important role in determining what rock types the magma body incorporated as xenoliths.

Incorporation of the pelitic quartzite into the magma occurred via brittle fracture along foliated layers, by dehydration melting reactions in muscovite and biotite-rich layers of the pelitic quartzite, or by a combination of the two processes. The pelitic quartzite is the only foliated unit in the May Lake screen, but foliated metavolcanic rocks in contact with the eastern margin of the Tuolumne Intrusive Suite experienced similar concordant separation and incorporation along metamorphic foliation (Fig. 4d).

Wall rock xenoliths are concentrated in a planar horizon (Fig. 2) oriented subparallel to the contact between the screen and the pluton. Surrounding many xenoliths in the horizon is a fine-grained, leucocratic, hybridized granodiorite that appears to be a mixture of granodiorite and felsic partial melt from the xenoliths (Fig. 4b). The hybridized granodiorite is restricted to within a few meters of visible pelitic material. The horizon suggests syn-emplacement disaggregation, dispersal, and partial melting of wall rock blocks by granodioritic magma that later hybridized.

Determining contaminants

The variability found in the hybridized granodiorite geochemical data, and specifically the bimodal K_2O trends (Figs. 6, 11), suggests incorporation of a minimum of two different contaminants. One contamination trend produced hybrid samples that have a positive correlation between K_2O and SiO_2. Bulk assimilation of the observed wall rocks in the screen (marble, calc-silicate rocks, quartzite, and pelitic quartzite) cannot produce the major-element variability seen in these high-K hybrids. Major-element data for these rocks suggest either selective assimilation of a rhyolitic composition partial melt derived from the wall rocks or bulk assimilation of a granitic composition igneous rock not present at the level of exposure. The second contamination trend has a negative correlation between K_2O and SiO_2. Major-element data for this trend fit either bulk assimilation of pure quartzite, selective assimilation of a low-K_2O partial melt derived from the wall rocks, or bulk assimilation of a trondhjemitic igneous rock not present at the level of exposure. Although bulk assimilation of igneous rocks at lower levels in the crust cannot be ruled out by the data, the close proximity of the hybridized granodiorite to the wall rock screen and xenoliths suggests a relationship between the metasedimentary rocks and the contamination of the granodiorite.

The low-K hybridized granodiorites have significant trace-element variability, including large variations in Th and LREE. Two samples (ML051.02 and ML061.36) have concentrations of Th and REE that are significantly higher than any granodiorite or quartzite sample. For these samples, hybridization was not a result of bulk assimilation of pure quartzite. The remaining low-K hybrids do not show this dramatic spike in Th or LREE and thus bulk assimilation of pure quartzite is plausible according to chemical analyses. However, if the low-K hybrids are trending towards one distinct contaminant, then the low-K hybrids with the largest chemical variability highlight the assimilation process and the low-K hybrids with mild chemical variability exemplify the same process cryptically. Overall, evidence for bulk assimilation of quartz is plausible in a few mildly hybridized samples.

Because selective assimilation of partial melts derived from metasedimentary wall rocks is the likely contamination process that produced both K_2O trends of hybridization (high-K and low-K) it is important to determine the parental wall rock for the partial melts. Partial melting generally results in a liquid with different chemistry than the original solid (Fig. 13). Because the pure quartzite and marble units are essentially monomineralic rocks, they are extremely limited in their ability to melt incongruently, and would only produce minimal volumes of partial melt. This restricts potential fertile source rocks

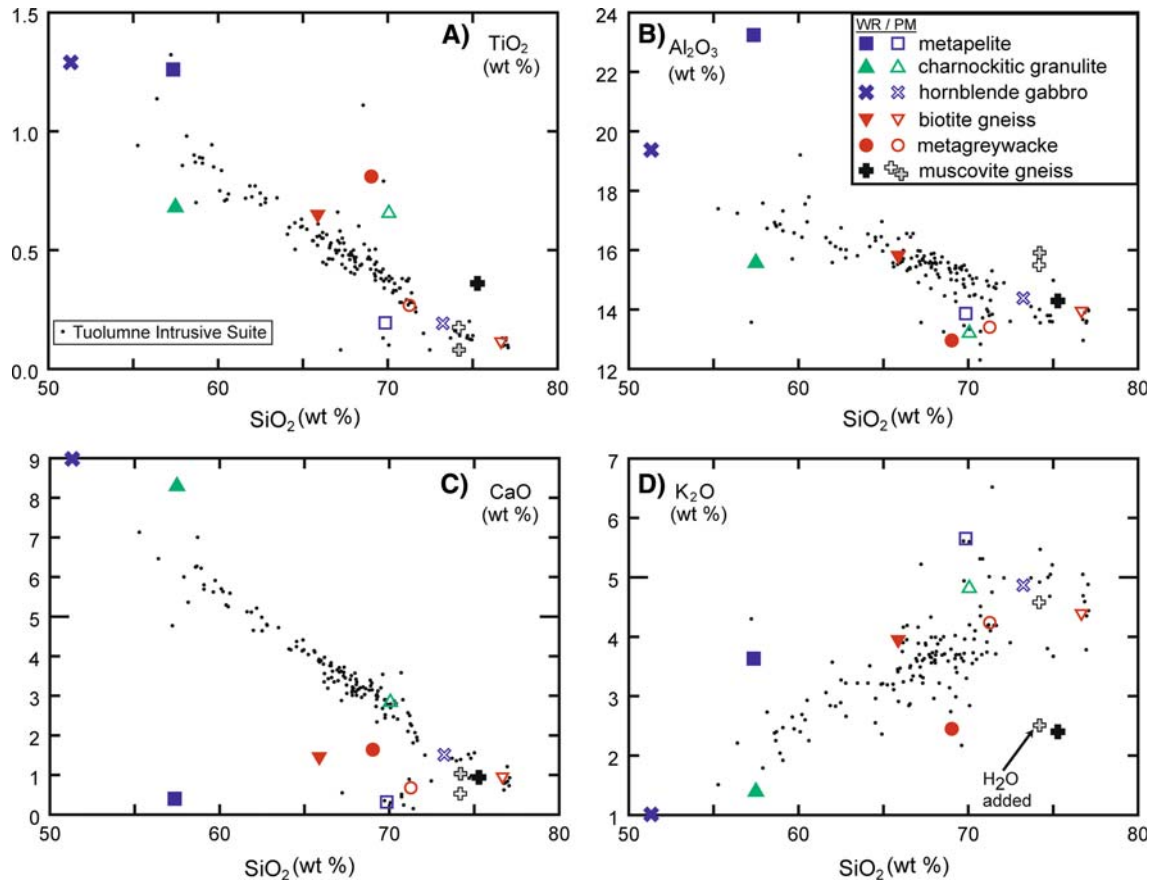

Fig. 13 Selected major-element variation diagrams of whole rock and melting experiment geochemistry. Melting data is plotted as an average of multiple melting experiments on one protolith. Melting data used in averages were as follows: metapelite at 7 kbar and 825°, 850°, 875°, 900°, and 950° (Patiño-Douce and Johnston 1991), charnockitic granulite at 6.9 kbar and 900°, 925°, 950°, and 1000° (Beard et al. 1993), hornblende gabbro MnO–Mn_3O_4 series of runs at 7 kbar and 825°, 850°, 875°, 900°, and 925° (Sisson et al. 2005), biotite gneiss at 3 kbar and 750 (x4), and 700 (x3) degrees (Holtz and Johannes 1991), metagreywacke at 3 kbar 805, 834, 853, and 875 (Montel and Vielzeuf 1997), muscovite schist at 6 and 10 kbar and temperatures from 700 to 900 divided into two groups based on presence of H_2O, all values reported were used (Patiño-Douce and Harris 1998). Data from the Tuolumne Intrusive Suite (Bateman et al. 1988; Gray et al. 2008) plotted as reference to igneous rock trend

from the screen that could produce enough partial melt to hybridize the adjacent granodiorite to the pelitic quartzite and the calc-silicate rocks.

Experimental partial melting studies (e.g. Holtz and Johannes 1991; Patiño-Douce and Johnston 1991; Montel and Vielzeuf 1997; Patiño-Douce and Harris 1998) of melt generation in pelitic rocks combined with geochemical studies of leucosomes in migmatites (e.g. Bea et al. 1994; Whitney and Irving 1994; Carrington and Watt 1995; Symmes and Ferry 1995; Zeng et al. 2005a; Fig. 1) provide detailed information on melting reactions that are likely to occur during contact metamorphism of pelitic material, and the range of compositions that will be produced from these partial melting reactions (Figs. 1, 13). Experimental studies and leucosome analyses consistently obtain high-K_2O (rhyolitic) initial partial melts that are indistinguishable from peraluminous leucogranite compositions (Montel and Vielzeuf 1997). However, some melting experiment products and leucosomes are low-K_2O (trondhjemitic) in composition (Fig. 1d).

Potassium variability in partial melts of a pelitic source can relate to the activity of H_2O, protolith variability, and degree of partial melting of the protolith. In order for the degree of partial melting to account for the two hybrid trends a trondhjemitic rock would be the likely source. Initial melting of a trondhjemite could yield a high-K partial melt and higher degrees of melting would yield a low-K partial melt. However, a spectrum of partial melt compositions would be expected depending on degree of melting and more hybridization trends would be seen. In addition, the lack of trondhjemitic rocks exposed in the Sierra Nevada batholith (Bateman 1992) suggests that variability in degree of partial melting was not the cause of the bimodal hybridization. Mineral variability in the pelitic

quartzite and changing H_2O activity during partial melting are both likely causes of the two distinct contamination trends.

The pelitic quartzite unit is chemically variable as illustrated by major-element geochemistry (Fig. 6). Compositional variability causes modal variability that can affect melting reactions in many ways. For example, when K-feldspar is a reactant along with plagioclase and quartz ± aluminosilicate, muscovite, and biotite, a rhyolitic (high-K) composition leucocratic melt is produced (Al-Rawi and Carmichael 1967). However, mineral composition and H_2O activity are intrinsically related owing to dehydration reactions during melting. Carrington and Watt (1995) suggested $H_2O/K_2O_{(melt)}$ in relation to $H_2O/K_2O_{(biotite)}$ controls whether K-feldspar is a reactant during melting. Low $H_2O/K_2O_{(melt)}$ relative to biotite causes K-feldspar to become a reactant during melting, creating a partial melt rich in K_2O, whereas high $H_2O/K_2O_{(melt)}$ relative to biotite causes K-feldspar to become a product during melting. Thus, the mineral assemblage plagioclase + quartz + K-feldspar + aluminosilicate + muscovite + biotite can produce either a trondhjemitic (low-K) partial melt during high H_2O activity or a rhyolitic/granitic (high-K) partial melt during low H_2O activity (Patiño-Douce and Harris 1998). As the activity of H_2O increases, the melting temperature decreases and plagioclase and quartz are consumed in greater proportion than muscovite because mica stability extends to lower temperatures (Patiño-Douce and Harris 1998).

Leucosomes of both varieties (high-K and low-K) can occur within the same migmatite complexes (Zeng et al. 2005a), suggesting that the activity of H_2O can vary within short distances in contact aureoles, perhaps owing to variability the CO_2 proportion in the fluid. Free CO_2 would be available due to degassing of $CaCO_3$ found in the marble and calc-silicate rocks of the metamorphic screen.

The high concentrations of Th and LREE in some of the low-K hybrids could be related to the high dissolution rate of monazite during fluid-present melting (Carrington and Watt 1995; Zeng et al. 2005b). Analysis of heavy mineral separates (Table 3) suggests that monazite is the mineral with the largest concentrations of Th and LREE in the pelitic quartzite. However, the granodiorite mineral separates showed uranothorite and allanite with the largest concentrations of Th and LREE, with the hybrid sample from within 10 cm of the pelitic quartzite containing more uranothorite and allanite than the uncontaminated granodiorite sample. It is probable that the high dissolution of monazite into the low-K partial melt increased the overall concentrations of LREE and Th in the adjacent hybridized magma, resulting in greater abundances of uranothorite and allanite.

Trace-element geochemistry of several of the high-K hybrids is consistent with only minor dissolution of trace phases (e.g. zircon and monazite) in the melt (Carrington and Watt 1995). The lack of significant REE contributions from trace phases to the whole-rock composition causes major phases to control the REE pattern. A depleted pattern with a positive Eu anomaly caused by the melting of K-feldspar is seen in three high-K hybrid samples and is consistent with the high-K leucosomes analyzed by Carrington and Watt (1995).

Major- and trace-element data suggest that both partial melts originated from the pelitic quartzite unit in the May Lake screen. However, we have not ruled out the potential contribution of a calc-silicate rock partial melt. Detailed chemical studies of mafic magmas in contact with calcareous wall rocks show that basaltic magmas can initiate partial melting of the wall rocks and selectively assimilate a calcium-rich liquid (Joesten 1977; Wenzel et al. 2002), but, similar to our findings, the magma contamination is limited in extent (<3 m; Joesten 1977), and restitic xenoliths are common (Preston et al. 1999). No calc-silicate rock xenoliths had rinds indicative of partial melting like the pelitic quartzite xenoliths. And although many of the hybridized samples are enriched in K_2O and/or Na_2O, none of the hybridized samples are enriched in CaO relative to the granodiorite.

Bulk or selective assimilation of marble and calc-silicate rocks was not observed in the plutons near May Lake and thus all incorporated calcareous material is visible as xenoliths. However, because marble and calc-silicate rocks make up a small percentage of the observed xenoliths near May Lake (<5%) and no large blocks of marble or calc-silicate rocks are observed, it is likely that little calcareous wall rock material entered the magma in any form. Because these calcareous rock types are common in the upper crust, their lack of incorporation into magma bodies inhibits the process of large-scale assimilation of metasedimentary sequences that contain marble or calc-silicate rock units.

Reconciling chemical mixing percentages

Calculated mixing percentages, from selected major-elements, of the hybridized samples cover a broad range of mixing between wall rock partial melt and magmatic (Kga) melt (Fig. 12). Major-element concentrations for Kga and two distinct partial melts from pelitic quartzite have restricted variability and provide quantifiable mixing proportions (Table 4). However, the calculated mixing percentages for the hybrid samples have no significant correlation with $^{87}Sr/^{86}Sr_{(i)}$ (Fig. 12) or $\varepsilon Nd_{(t)}$. The low correlation between calculated mixing percentages and $^{87}Sr/^{86}Sr_{(i)}$ and $\varepsilon Nd_{(t)}$ relates to: (1) the high-isotopic variability of the quartzite samples ($^{87}Sr/^{86}Sr_{(i)} = 0.7062$ to

Table 4 Weighted least squares analyses of mixing

Oxide	Kga	Partial melt	Low-K hybridized granodiorite					Partial melt	High-K hybridized granodiorite						Weights (1/σ)
	ML061.63	Low-K	ML051.02	ML051.18	ML061.25	ML061.36	ML061.60	High-K	ML051.08	ML061.26	ML061.28	ML061.30	ML061.38	ML061.40	
SiO_2	61.54	72.68	77.86	64.38	66.56	75.68	72.59	72.89	66.62	62.06	76.69	72.00	64.88	67.49	4.9
TiO_2	0.76	0.26	0.33	0.86	0.85	0.39	0.41	0.19	0.52	0.785	0.14	0.19	0.98	0.59	88.5
Al_2O_3	16.25	15.46	11.17	16.54	15.67	12.49	13.93	14.47	15.73	16.74	12.81	15.43	14.97	14.78	5.2
MgO	2.43	0.68	0.73	2.45	1.95	1.05	1.22	0.46	1.72	2.49	0.34	0.50	2.74	1.61	17.5
CaO	4.78	2.78	2.55	4.39	4.10	2.64	3.64	1.16	3.86	5.01	1.90	2.77	3.23	3.07	24.9
Na_2O	3.28	4.50	2.53	3.41	3.40	2.13	3.12	2.85	3.33	3.46	2.65	3.43	2.23	2.93	15.9
K_2O	3.20	0.91	1.61	2.28	2.10	2.05	1.17	5.20	3.81	3.04	4.36	4.03	3.43	3.60	25.2
Partial melt component			1.32	0.20	0.41	1.07	0.90		0.33	−0.05	1.09	0.67	0.35	0.50	
Kga component			−0.36	0.81	0.59	−0.09	0.09		0.69	1.07	−0.07	0.37	0.63	0.50	

Fe oxide concentrations omitted due to the variability of technique and reporting style

0.7741 and $\varepsilon Nd_{(t)} = -5.1$ to -23.7), (2) isotopic disequilibrium (Knesel and Davidson 1996; Zeng et al. 2005a) during partial melting of the pelitic material, and (3) modal segregation seen in the outer portion of the pluton, which can disguise the original contamination by segregating minerals, some with drastically different distribution coefficients for Sr and Nd (Gromet and Silver 1983).

Mixing hyperbolas (Fig. 12) between Kga and different quartzite samples, with reasonable Sr concentrations for the partial melts (Bea et al. 1994), illustrate the high variability of $^{87}Sr/^{86}Sr_{(i)}$ that should be expected during such partial melting/mixing processes. However, the mixing hyperbolas shown are non-quantifiable paths of mixing because multiple mixing path solutions for each hybrid sample exist. Variability in the protolith, disequilibrium melting, and modal control on trace-element concentrations makes the isotopic mixing relationships complicated and difficult to quantify accurately. Thus, the major-element mixing percentages give the more interpretable results of mixing and show a complete spectrum of mixing between Kga and both partial melts.

Limits of contamination in the Tuolumne Intrusive Suite

The gradational Sr and Nd isotopic variation toward more crustal ratios in the core led Kistler et al. (1986) to suggest a two-component system consisting of a mafic magma ($SiO_2 = 48.0$ wt.%, $Sr_i = 0.7047$, $Nd_i = 0.51269$) and felsic magma ($SiO_2 = 73.3$ wt.%, $Sr_i = 0.7068$, $Nd_i = 0.51212$) that mixed in varied proportions and rose through the upper crust and solidified as the Tuolumne Intrusive Suite. Gray et al. (2008) modified the isotopic values for the mafic component to match mantle xenoliths found in the Sierra Nevada batholith. This new two-component system could account for all units of the TIS except Kga. They suggested a connection between the older 102 Ma granitoids (Sentinel and Yosemite Valley; Fig. 9) in the area and Kga. Whether there is one or two felsic components to the suite does not change the point that both models use a basaltic magma and lower crustal, felsic melt(s) to produce the plutonic rocks of the suite. These models do not include contamination by crustal material in the upper crust at the level of emplacement, but with identification of wall rock-contaminated plutonic rocks near May Lake we can use geochemical data to test whether in situ wall rock contamination caused or added to the crustal isotopic values of the interior units.

The length scale of in situ contamination along the side of the suite near May Lake is restricted to within 2 m of wall rock material (Fig. 10). This thin rind of contamination in the outer portion of the suite can be interpreted in two ways: (1) contamination is localized at contacts

between fertile wall rock and magma, and similar roof contacts in the central portions of the suite are no longer preserved owing to erosion or (2) identifiable chemical hybridization is only preserved at the outer contacts when and where the magma system was thermally immature, and the inner units, over time, homogenized their assimilated material such that remnants of that process are preserved in the overall elemental and isotopic gradation from margin to core in the Tuolumne Intrusive Suite (Fig. 10).

If selective assimilation of wall rock at the level of emplacement only occurred as a rind surrounding the suite, we can establish an upper limit on volume transferred from wall rock to pluton. We calculated the upper limit volume percent of both Kga and the entire suite that could be wall rock material by placing a 2-m wide rind of 100% wall rock partial melt along the outer contacts with wall rock. The $\sim$60 km^2 Kga (western, outer unit only) would thus have 0.2 area % wall rock contamination. Assuming a rectangular intrusion with roof and floor contacts contributing the same 2 m rind of contamination, and a minimum pluton thickness of 1 km (based on present relief of plutonic suite), selective assimilation could contribute 0.6 volume % of Kga. For the entire Tuolumne Intrusive Suite, selective assimilation could contribute 0.44 volume % of a 1-km thick suite. Thickening the suite decreases the percentage with a 2-km thick suite having 0.24 volume % wall rock partial melt, and a 5-km thick suite having 0.12 volume % wall rock partial melt.

If selective assimilation of wall rock was pervasive during emplacement of the inner units of the Tuolumne Intrusive Suite and the increasingly crustal isotopic ratios of inner units relate to in situ wall rock contamination, a much larger and potentially unrealistic volume % wall rock partial melt is necessary. The major-element variability of the inner units is consistent with both Kga and the high-K partial melts, but there is no chemical evidence of assimilation of a low-K partial melt in the interior of the suite. In addition, if in situ selective assimilation is the cause of the isotopic variability, one would expect greater Sr and Nd isotopic variability in the interior of the suite due to: (1) the wall rock dependence of partial melting, and (2) the high variability in Sr and Nd isotopic ratios in the partial melts, and this scattered variability is not observed.

The systematic change in isotopic data across the entire suite (Kistler et al. 1986; Gray et al. 2008; Figs. 9, 10) and the lack of trondhjemitic (low-K) compositions in the interior units suggests that the elemental and isotopic variability in the TIS relates to an earlier stage in magma generation where rhyolitic (high-K) melt was the predominant felsic component. A migration of the source magmatism in the lower crust under the Sierra Nevada batholith during petrogenesis of the inner units of the suite (Gray et al. 2008), which mimics other concentrically zoned suites (e.g. Whitney Intrusive Suite; Coleman and Glazner 1997) seems a probable explanation for the systematic variation in geochemistry. Thus, the restricted contamination from the metasedimentary rocks probably existed along contacts between the inner units and fertile roof rocks, but this contamination rind has been eroded.

Conclusions

1. The predominant observable contaminant in the outer portion of the granodiorite of Glen Aulin is pelitic quartzite, which is the only foliated metasedimentary rock unit in the adjacent May Lake metamorphic screen. This rock type makes up approximately 90% of observed xenoliths.
2. Xenoliths are exceedingly rare in the Tuolumne Intrusive Suite (<0.0001% by area; Glazner and Bartley 2008), but are found in some abundance (locally up to 10% of selected 10 × 10 m area) in a xenolith-rich horizon subparallel to the contact. However, outside of this horizon, xenoliths make up $\ll$1% of the exposed area, even adjacent to the contact with the metamorphic screen.
3. Major-element, trace-element, and radiogenic isotopic data suggest localized contamination of the pluton within 2 m of the contact with wall rock material.
4. No significant bulk or selective assimilation of marble or calc-silicate rocks occurred during emplacement of the granodiorite of Glen Aulin and such rocks make up only a small fraction (<10%) of observed xenoliths.
5. The contamination path is bimodal, with some of the hybridized samples trending toward high SiO_2 ($\sim$75 wt.%) and high K_2O ($\sim$5 wt.%) and the rest trending toward high SiO_2 ($\sim$75 wt.%) and low K_2O (<1 wt.%).
6. Major-element and trace-element data suggest that bulk assimilation of wall rock was insignificant during emplacement of the Tuolumne Intrusive Suite and the localized contaminants are partial melts selectively assimilated from the pelitic quartzite (one with high-K_2O and the other with low-K_2O).
7. Geochemical trends of contamination in the hybridized samples are consistent with data from leucosomes in migmatites which suggests that at least two main melting reactions produce two chemically distinct partial melts, one high-K_2O and one low-K_2O.
8. Assimilation of wall rock is not a significant space conserving mechanism for the emplacement of the Tuolumne Intrusive Suite because of the spatially restricted contamination of the plutonic rocks.

Acknowledgements This work has been supported by grants from the National Science Foundation (EAR-9814789, EAR-0336070, and EAR-0538129) and by a student grants from the University of California's White Mountain Research Station, and the University of North Carolina Martin and Bartlett Funds. The manuscript was greatly improved by incorporation of suggestions from reviewers James Beard, an anonymous reviewer and editor Jon Blundy. Our work greatly benefited by field time spent with numerous colleagues and students, including John Bartley, Breck Johnson, Jesse Davis, Walt Gray, John Templeton, and Sam Coleman. We gratefully acknowledge generous cooperation and logistical support from the U.S. National Park Service and U.S. Geological Survey, in particular Jan van Wagtendonk, Peggy Moore, and Greg Stock. We also want to thank Jeff Grossman for his help with the large dataset of geochemistry we used in several figures.

References

Al-Rawi Y, Carmichael ISE (1967) A note on the natural fusion of granite. Am Mineral 52:1806–1814

Baedecker PA, Grossman JN, Buttleman KP (1998) National geochemical data base, PLUTO geochemical data base for the United States. US Geological Survey CD-ROM

Barnes CG, Dumond G, Yoshinobu AS, Prestvik T (2004) Assimilation and crystal accumulation in a mid-crustal magma chamber: the Sausfjellet pluton, north-central Norway. Lithos 75:389–412. doi:10.1016/j.lithos.2004.04.036

Barnes CG, Prestvik T, Sundvoll B, Surratt D (2005) Pervasive assimilation of carbonate and silicate rocks in the Hortavær igneous complex, north-central Norway. Lithos 80:179–199. doi:10.1016/j.lithos.2003.11.002

Bateman PC (1992) Plutonism in the central part of the Sierra Nevada Batholith, California. US Geological Survey Professional Paper, Report P 1483, p 186

Bateman PC, Chappell BW, Kistler RW, Peck DL, Busacca AJ (1988) Tuolumne Meadows Quadrangle, California; analytic data, US Geological Survey Bulletin, Report: B 1819 8755-531X

Bea F, Pereira MD, Stroh A (1994) Mineral/leucosome trace-element partitioning in a peraluminous migmatite (a laser ablation-ICP–MS study). Chem Geol 117:291–312. doi:10.1016/0009-2541(94)90133-3

Beard JS, Abitz RJ, Lofgren GE (1993) Experimental melting of crustal xenoliths from Kilbourne Hole, New Mexico and implications for the contamination and genesis of magmas. Contrib Mineral Petrol 115:88–102. doi:10.1007/BF00712981

Beard JS, Ragland PC, Crawford ML (2005) Reactive bulk assimilation: a model for the crust-mantle mixing in silicic magmas. Geology 33:681–684. doi:10.1130/G21470.1

Bhadra S, Das S, Bhattacharya A (2007) Shear zone-hosted migmatites (Eastern India): the role of dynamic melting in the generation of REE-depleted felsic melts, and implications for disequilibrium melting. J Petrol 48:435–457. doi:10.1093/petrology/egl066

Bowen NL (1928) The evolution of igneous rocks. Princeton University Press Princeton, New Jersey

Burchfiel BC, Davis GA (1972) Structural framework and evolution of the southern part of the Cordilleran orogen, western United States. Am J Sci 272:97–118

Carrington DP, Watt GR (1995) A geochemical and experimental study of the role of K-feldspar during water-undersaturated melting of metapelites. Chem Geol 122:59–76. doi:10.1016/0009-2541(95)00046-O

Clarke DB, Henry AS, White MA (1998) Exploding xenoliths and the absence of "elephants' graveyards" in granite batholiths. J Struct Geol 20:1325–1343. doi:10.1016/S0191-8141(98)00082-0

Coleman DS, Glazner AF (1997) The Sierra Crest magmatic event: rapid formation of juvenile crust during the late Cretaceous in California. Int Geol Rev 39:768–787

Coleman DS, Gray W, Glazner AF (2004) Rethinking the emplacement and evolution of zoned plutons: Geochronologic evidence for incremental assembly of the Tuolumne Intrusive Suite, California. Geol Soc Am Bull 32:433–436

Coleman DS, Glazner AF, Bartley JM, Law RD (2005) Incremental assembly and emplacement of Mesozoic plutons in the Sierra Nevada and White and Inyo Ranges, California, Geological Society of America Field Forum Field Trip Guide (Rethinking the assembly and evolution of plutons: Field tests and perspectives, 7–14 October 2005) p 55

Dumond G, Yoshinobu AS, Barnes CG (2005) Midcrustal emplacement of the Sausfjellet Pluton, central Norway; ductile flow, stoping, and in situ assimilation. Geol Soc Am Bull 117:383–395. doi:10.1130/B25464.1

Dungan MA (2005) Partial melting at the earth's surface: implications for assimilation rates and mechanisms in subvolcanic intrusions. J Volcanol Geotherm Res 140:193–203. doi:10.1016/j.jvolgeores.2004.07.021

Glazner AF (2007) Thermal limitations on incorporation of wall rock into magma. Geology 35:319–322. doi:10.1130/G23134A.1

Glazner AF, Bartley JM (2006) Is stoping a volumetrically significant pluton emplacement process? Geol Soc Am Bull 118:1185–1195. doi:10.1130/B25738.1

Glazner AF, Bartley JM (2008) Reply to comments on "Is stoping a volumetrically significant pluton emplacement process?". Geol Soc Am Bull 120:1082–1087. doi:10.1130/B26312.1

Glazner AF, Mills RD, Coleman DS (2008) Selective vs. bulk assimilation and the restricted chemical variability of igneous rocks. Goldschmidt Conference Abstracts (in press)

Gray W (2003) Chemical and thermal evolution of the Late Cretaceous Tuolumne Intrusive Suite, Yosemite National Park, California, PhD thesis, Chapel Hill. University of North Carolina, North Carolina, p 202

Gray W, Glazner AF, Coleman DS, Bartley JM (2008) Long-term geochemical variability of the Late Cretaceous Tuolumne Intrusive Suite, Central Sierra Nevada, California. Geological Society of London. Spec Publ 304:183–201

Gromet LP, Silver LT (1983) Rare earth element distributions among minerals in a granodiorite and their petrogenetic implications. Geochim Cosmochim Acta 47:925–939. doi:10.1016/0016-7037(83)90158-8

Hinchey AM, Carr SD (2006) The S-type Ladybird leucogranite suite of southeastern British Columbia: Geochemical and isotopic evidence for a genetic link with migmatite formation in the North American basement gneisses of the Monashee complex. Lithos 90:223–248. doi:10.1016/j.lithos.2006.03.003

Holtz F, Johannes W (1991) Genesis of peraluminous granites I. Experimental investigation of melt compositions at 3 and 5 kb and various H_2O activities. J Petrol 32:935–958

Huber NK, Bateman PC, Wahrhaftig C (1989) Geologic map of Yosemite National Park and vicinity, California, US Geological Survey Map I-1874, scale 1:125,000

Joesten R (1977) Mineralogical and chemical evolution of contaminated igneous rocks at a gabbro-limestone contact, Christmas Mountains, Big Bend region, Texas. Geol Soc Am Bull 88:1515–1529. doi:10.1130/0016-7606(1977)88<1515:MACEOC>2.0.CO;2

Johnson TE, Hudson NFC, Droop GTR (2003) Evidence for a genetic granite-migmatite link in the Dalradian of NE Scotland. J Geol Soc Lond 160:447–457. doi:10.1144/0016-764902-069

Jung S, Mezger K, Masberg P, Hoffer E, Hoernes S (1998) Petrology of an intrusion-related high-grade migmatite: implications for partial melting of metasedimentary rocks and leucosome-

forming processes. J Metamorph Geol 16:425–445. doi:10.1111/j.1525-1314.1998.00146.x

Kistler RW, Chappell BW, Peck DL, Bateman PC (1986) Isotopic variations in the Tuolumne Intrusive Suite, central Sierra Nevada, California. Contrib Mineral Petrol 94:205–220. doi:10.1007/BF00592937

Knesel KM, Davidson JP (1996) Isotopic disequilibrium during melting of granite and implications for crustal contamination of magmas. Geology 24:243–246. doi:10.1130/0091-7613(1996)024<0243:IDDMOG>2.3.CO;2

Lahren MM, Schweickert RA, Mattinson JM, Walker JD (1990) Evidence of uppermost Proterozoic to Lower Cambrian miogeoclinal rocks and the Mojave-Snow Lake fault: Snow Lake pendant, central Sierra Nevada, California. Tectonics 9:1585–1608. doi:10.1029/TC009i006p01585

Le Maitre RW (2002) Igneous rocks: a classification and glossary of terms, 2nd edn. Cambridge University Press, Cambridge

McBirney AR, Taylor HP, Armstrong RL (1987) Paricutin re-examined: a classic example of crustal assimilation in calc-alkaline magma. Contrib Mineral Petrol 95:4–20. doi:10.1007/BF00518026

Miller JS, Glazner AF, Walker JD, Martin MW (1995) Geochronologic and isotopic evidence for Triassic-Jurassic emplacement of the eugeoclinal allochthon in the Mojave Desert region, California. Geol Soc Am Bull 107:1441–1457. doi:10.1130/0016-7606(1995)107<1441:GAIEFT>2.3.CO;2

Milord I, Sawyer EW, Brown M (2001) Formation of Diatexite Migmatite and Granite Magma during anatexis of semi-pelitic metasedimentary rocks: an example from St Malo, France. J Petrol 42:487–505. doi:10.1093/petrology/42.3.487

Montel JM, Vielzeuf D (1997) Partial melting of metagreywackes, Part II. Compositions of minerals and melts. Contrib Mineral Petrol 128:176–196. doi:10.1007/s004100050302

Patiño-Douce AE, Harris N (1998) Experimental constraints on Himalayan anatexis. J Petrol 39:689–710. doi:10.1093/petrology/39.4.689

Patiño-Douce AE, Johnston AD (1991) Phase equilibria and melt productivity in the pelitic system: implications for the origin of peraluminous granitoids and aluminous granulites. Contrib Mineral Petrol 107:202–218. doi:10.1007/BF00310707

Preston RJ, Dempster TJ, Bell BR, Rogers G (1999) The petrology of mullite-bearing peraluminous xenoliths: implications for contamination processes in basaltic magmas. J Petrol 40:549–573. doi:10.1093/petrology/40.4.549

Ratajeski K (1999) Field, geochemical and experimental study of mafic to felsic plutonic rocks associated with the Intrusive Suite of Yosemite Valley, California, PhD thesis, Chapel Hill. North Carolina, University of North Carolina, p 196

Roberts D, Nordgulen Ø, Melezhik V (2007) The Uppermost Allochthon in the Scandinavian Caledonides: from a Laurentian ancestry through Taconian orogeny to Scandian crustal growth on Baltica. In: Hatcher RD, Carlson MP, McBride JH, Martinez Catalan JR (eds) 4-D framework of continental crust. Geological Society of America Memoir, vol 200, pp 357–377

Rose RL (1957) Andalusite and corundum bearing pegmatities in Yosemite National Park, California. Am Mineral 42:635–647

Saito S, Makoto A, Nakajima T (2007) Hybridization of a shallow 'I-type' granitoid pluton and its host migmatite by magma-chamber wall collapse: the Tokuwa Pluton, Central Japan. J Petrol 48:79–111. doi:10.1093/petrology/egl055

Sawyer EW (1987) The role of partial melting and fractional crystallization in determining discordant migmatite leucosome compositions. J Petrol 28:445–473

Schweickert RA, Lahren MM (1991) Age and tectonic significance of metamorphic rocks along the axis of the Sierra Nevada batholith: a critical reappraisal. In: Cooper J, Stevens C (eds) Paleozoic paleography of the western United States-II, Society for Sedimentary Geology. Pac Sect 67:653–676

Sisson TW, Ratajeski K, Hankins WB, Glazner AF (2005) Voluminous granitic magmas from common basaltic sources. Contrib Mineral Petrol 148:635–661. doi:10.1007/s00410-004-0632-9

Sun SS, McDonough WF (1989) Chemical and isotopic systematics of oceanic basalts; implications for mantle composition and processes. Geol Soc Lond Spec Publ 42:313–345

Symmes GH, Ferry JM (1995) Metamorphism, fluid flow and partial melting in pelitic rocks from the Onawa contact aureole, Central Maine, USA. J Petrol 36:587–612

Taylor RZ (2003) Structure and stratigraphy of the May Lake interpluton screen, Yosemite National Park, California, MS thesis, Chapel Hill. University of North Carolina, North Carolina, p 55

Wenzel T, Baumgartner LP, Brugmann GE, Konnikov EG, Kislov EV (2002) Partial melting and assimilation of dolomitic xenoliths by mafic magma: the Ioko-Dovyren intrusion (North Baikal Region, Russia). J Petrol 43:2049–2074. doi:10.1093/petrology/43.11.2049

Whitney DL, Irving AJ (1994) Origin of K-poor leucosomes in a metasedimentary migmatite complex by ultrametamorphism, syn-metamorphic magmatism and subsolidus processes. Lithos 32:173–192. doi:10.1016/0024-4937(94)90038-8

Zeng L, Saleeby JB, Ducea M (2005a) Geochemical characteristics of crustal anatexis during the formation of migmatite at the Southern Sierra Nevada, California. Contrib Mineral Petrol 150:386–402. doi:10.1007/s00410-005-0010-2

Zeng L, Asimow PD, Saleeby JB (2005b) Coupling of anatectic reactions and dissolution of accessory phases and the Sr and Nd isotope systematic of anatectic melts from a metasedimentary source. Geochim Cosmochim Acta 69:3671–3682. doi:10.1016/j.gca.2005.02.035